Geomechanics and Engineering, *Vol. 42, No. 3 (2025) 207-220*
https://doi.org/10.12989/gae.2025.42.3.207

Prediction and control measures of water inflow for subsea tunnels

Yunjuan Chen[1,2a], Mengyue Liu[*3], Zongqing Zhou[3b], Mengzhen Su[1c] and Shangqu Sun[4d]

[1]*School of Civil Engineering, Shandong Jianzhu University, Jinan 250101, China*
[2]*Key Laboratory of Building Structural Retrofitting and Underground Space Engineering, Ministry of Education, Shandong Jianzhu University, Jinan 250101, China*
[3]*School of Qilu Transportation, Shandong University, Jinan 250002, China*
[4]*College of Civil Engineering and Architecture, Shandong University of Science and Technology, Jinan 250002, China*

(*Received August 28, 2023, Revised June 10, 2025, Accepted June 17, 2025*)

Abstract. Predicting water inflow and optimizing waterproofing-drainage systems are critical for subsea tunnel safety. This study addresses the limitations of static parameter-based models by proposing a dynamic analytical formula for water inflow prediction, integrating tunnel depth, hydraulic head, and lining permeability using complex variable functions and Darcy's law. Additionally, three-dimensional numerical simulations were conducted to evaluate the stability and pore water pressure distribution of the tunnel in land section, sea section, and land-sea transition section with fully encapsulated or half-encapsulated waterproofing-drainage schemes. Key findings include: the half-encapsulated system reduced lining deformation by 15-20% in the land section, offering a cost-effective solution; pore water pressure in the sea section remained below 0.5 MPa (excluding class IV/V zones), recommending a fully encapsulated system with pressure-relief valves; and elevated pore water pressure (up to 0.42 MPa) at the land-sea interface necessitated adaptive drainage measures. While the analytical formula and numerical simulations address distinct aspects of tunnel design (water inflow prediction and structural stability), their combined insights provide a holistic framework for optimizing subsea tunnel systems under dynamic hydraulic conditions.

Keywords: deformation; pore water pressure; subsea tunnel; water inflow; waterproofing and drainage solutions

1. Introduction

With the development of the economy and society, the demand for cross-sea transportation has been increasing. Subsea tunnels, due to their advantages such as being unaffected by weather conditions, have been widely utilized. Subsea tunnels are usually deeply buried beneath the seabed and are subject to the combined effects of rock mass self-weight and constant hydraulic head. Issues such as sudden water inflow into the tunnel and excessive water pressure behind the lining are more prominent (Nilsen 2014, Shin *et al.* 2011, Aalianvari A 2017). Considering the characteristics of different sections, it is crucial to determine the water pressure behind the lining and predict the amount of water inflow into the tunnel (Golian *et al.* 2018). This is essential for establishing reasonable and feasible waterproofing and drainage systems to ensure the safety and stability of the tunnel (Mohammad Reza Zareifard 2018, Dammyr *et al.* 2014, Li *et al.* 2021).

Numerous scholars have conducted extensive research on predicting water inflow in tunnels (Farhadian *et al.* 2019). Ying *et al.* (2018) derived a semi-analytical solution for inflow inside tunnel linings in semi-infinite aquifers based on conformal mapping theory. Zou *et al.* (2020) study investigated water pressure and groundwater inflow distribution in a circular tunnel buried in a half-infinite aquifer with constant head and pressure conditions, utilizing coordinate transformation to simplify calculations. (Kolymbas *et al.* 2007, Butscher 2012) derived analytical solution for seepage in circular tunnels under the assumption of steady-state groundwater flow. (Park *et al.* 2008, Ming *et al.* 2010, Arjnoi *et al.* 2009) compared and studied the analytical solution of tunnel seepage fields with equal hydraulic head and equal water pressure boundaries around the tunnel. Pan *et al.* (2022) explores excavation damage zone impact on tunnel water inflow, with analytical solutions validated against finite element results. Li (2017) established a prediction model for tunnel water inflow based on nonlinear regression Gaussian equations and applied it. Zhu *et al.* (2019) derived analytical solutions for steady-state seepage field water inflow in parallel double-line tunnels using Darcy's law and the principle of mass conservation, employing conformal transformation and superposition methods. Zhang *et al.* (2020), focusing on the Qingdao Subsea Tunnel, proposed a water inflow prediction and analysis method based on the principle of superposition by combining theoretical analysis, numerical simulation and on-site monitoring.

The forms of drainage in tunnels mainly include complete sealing without discharge, combined sealing and discharge (limited discharge), and complete discharge. Li *et al.* (2012) proposed the concept of high water pressure and emphasized the need for adopting different drainage

*Corresponding author, Master
E-mail: liuyuximeng@163.com
[a]Professor
[b]Professor
[c]Master Candidate
[d]Professor

ISSN: 2005-307X (Print), 2092-6219 (Online)

solutions according to local conditions. Zhang *et al.* (2022) conducted a comparative analysis of various drainage design schemes, including complete sealing, semi-enclosure, and limited discharge, analyzing the distribution laws of the seepage field and displacement field of the surrounding rock mass in subsea tunnels, and optimizing the design of drainage solutions. (Wang *et al.* 2007, Wang *et al.* 2012, Xiuying *et al.* 2008) proposed the critical groundwater level as a principle for determining drainage measures for subsea tunnels and analyzed the distribution laws of water pressure behind the tunnel lining under different drainage conditions through indoor model experiments. Zhang *et al.* (2019) proposed a new concept for actively controlled drainage design with the core principle of "sealing water and limiting discharge" to address the contradiction between drainage control and structural water load in subsea tunnels.

Currently, most studies on water inflow in subsea tunnels are based on static parameters such as tunnel radius and seawater depth, lacking research on the relationship between water inflow and dynamic parameters (Li *et al.* 2017). Against this backdrop, relevant research has preliminarily established the correlation between dynamic parameters such as water inflow and lining water pressure. It is worth emphasizing that predicting water inflow using lining water pressure has significant advantages. Firstly, it has the property of dynamic real-time monitoring, which can better adapt to actual changes. Secondly, lining water pressure is easy to measure, and accurate values can be obtained on-site, effectively reflecting the actual situation. Thirdly, clarifying the relationship between lining water pressure and water inflow helps in the overall design of subsea tunnel waterproofing and drainage. It enables macroscopic control, improves the scientificity and rationality of the design, and provides strong support for the safe and stable operation of subsea tunnel projects. This paper preliminarily establishes the correlation between water inflow and dynamic parameters. Based on the Shantou Bay Subsea Tunnel, different drainage systems are adopted for different sections, and the displacement and pore water pressure distribution law of the tunnel lining structure are studied to provide guidance for the design of subsea tunnel drainage systems.

2. Project overview

The Shantou Bay Subsea Tunnel is located within the territory of Shantou City, Guangdong Province, China. The total length of the section using mining method is 6762 m, consisting of a 5636 m land section, and a 1126 m sea section. It is a dual-lane single-tube tunnel, with a with a substantial construction volume construction volume, classified as a key controlled tunnel project. It is the first 350 km/h high-speed railway subsea tunnel in China and in the world. The geological profile of the tunnel project is shown in Fig. 1.

The tunnel entrance is located in a mountainous hilly area with significant terrain variations. The tunnel mainly passes through hilly terrain, with the rock primarily

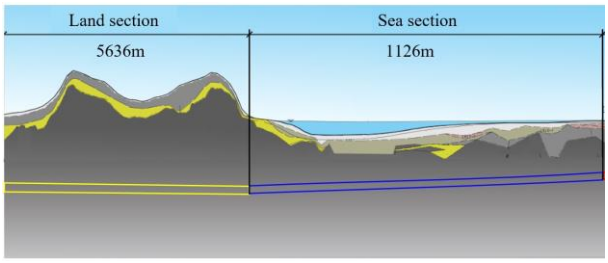

Fig. 1 Geological profile of the Shantou Bay Subsea Tunnel project

consisting of intrusive granite from the Yanshan period. The rock near the tectonic sections is relatively fragmented and hard. The tunnel passes through several faults, labeled F0~F12, with developed joint fissures, fragmented rock mass, and uneven distribution of rock layers. The surrounding rock mass is classified as class II, III, IV, and V.

The city of Shantou, where the tunnel is located, borders the South China Sea and is characterized by abundant sources of water vapor, high precipitation intensity, and plentiful rainfall. The surface water in the land section is mainly composed of streams and reservoirs, with a significant amount of surface runoff. During tunnel excavation, the rock mass cracks open, making it easier for water from reservoirs to infiltrate the tunnel through micro-fractures in the rock. In the sea section, the surface water is primarily seawater, and the groundwater consists of fractured bedrock water and Quaternary pore water, which are relatively well developed.

3. Derivation of the water inflow prediction formula for subsea tunnel

Assuming the surrounding rock is a homogeneous and isotropic porous medium, the seepage within the rock follows Darcy's law, and the lining of the tunnel allows for uniform water seepage during drainage.

Assuming that H_w represents the distance from the groundwater level to the seabed, H represents the depth from the center of the tunnel to the seabed, r_1 is the inner diameter of the tunnel lining, r_2 is the outer diameter of the tunnel lining, h_1 represents the hydraulic head at the inner wall of the lining, h_2 represents the hydraulic head at the outer wall of the lining, k_1 is the permeability coefficient of the lining, and k_2 is the permeability coefficient of the surrounding rock. The computational model for the seepage field of the subsea tunnel can be seen in Fig. 2.

Considering the symmetry in the surrounding rock region, half of the structure can be analyzed and calculated. The computational model for the seepage in the tunnel's surrounding rock region is shown in Fig. 3.

Based on the mapping functions (Huang *et al.* 2009, Pan 2004), the half-space region in the Z-plane can be mapped to a rectangular region in the ζ-plane. φ_e and φ_w represent the potential functions along the edges AB and CD, respectively.

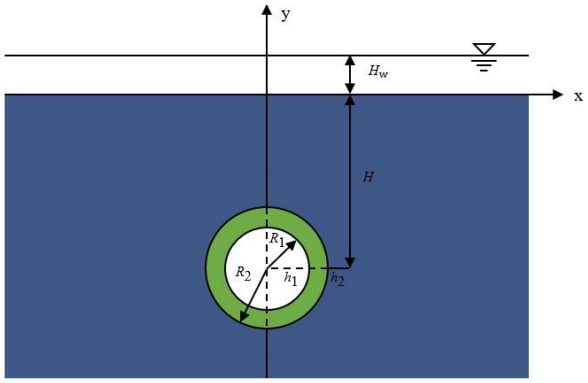

Fig. 2 Computational model for the seepage field in the subsea tunnel

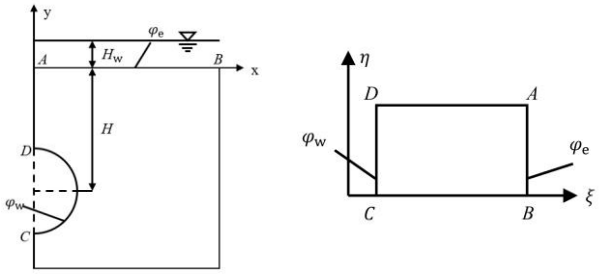

(a) Half-space region in the Z-plane (b) Rectangular region in the ζ-plane

Fig. 3 Computational model for the seepage in the tunnel's surrounding rock region

$$z=x+iy \tag{1}$$

$$w=u+iv\frac{z+i\sqrt{H^2-r_2^2}}{z-i\sqrt{H^2-r_2^2}} \tag{2}$$

$$\zeta=\xi+i\eta=\frac{Q}{2\pi}\ln w=\frac{Q}{2\pi}\ln(u+iv) \tag{3}$$

The boundary condition at the seabed is y=0

$$\ln\frac{\sqrt{x^2+\left(y+\sqrt{H^2-r_2^2}\right)^2}}{\sqrt{x^2+\left(y-\sqrt{H^2-r_2^2}\right)^2}}=0 \tag{4}$$

The boundary condition around the tunnel is

$$x^2+\left(y+\sqrt{H^2-r_2^2}\right)^2=r_2^2$$

$$\ln\frac{\sqrt{x^2+\left(y+\sqrt{H^2-r_2^2}\right)^2}}{\sqrt{x^2+\left(y-\sqrt{H^2-r_2^2}\right)^2}}=2\ln\left[\frac{H}{r_2}-\sqrt{\left(\frac{H}{r_2}\right)^2-1}\right] \tag{5}$$

According to the theory of complex variables, the potential function $\phi(\xi,\eta)$ and the stream function $\psi(\xi,\eta)$ in the ζ-plane satisfy the Laplace equation. By combining the boundary conditions and performing inverse transformations, the potential function and the stream function in the Z-plane can be obtained. Ultimately, the formula for calculating the seepage flow per meter of the tunnel's periphery is derived as follows

$$Q_1=\frac{2\pi k_2(H_w-h_2)}{\ln\left[\frac{H}{r_2}-\sqrt{\left(\frac{H}{r_2}\right)^2-1}\right]} \tag{6}$$

In the equation, Q_1 represents the water inflow per meter of the tunnel's surrounding rock.

The subsea tunnel is situated in a stable seepage field, where water flow is steady and there is an infinite water supply. Therefore, based on Darcy's law, we can deduce that the flow passing through a certain cross-section is given by

$$Q=2\pi rv=2\pi k\frac{dh}{dr} \tag{7}$$

Due to the difference in hydraulic head between the inner and outer boundaries of the lining, by integrating the variables in Eq. (7), the water inflow per meter through the lining can be obtained as Q_2 as follows

$$Q_2=2\pi k_1\frac{h_2-h_1}{\ln\frac{r_2}{r_1}} \tag{8}$$

Since the flow is the same at different sections of the subsea tunnel, that is, $Q_1=Q_2$, by combining Eqs. (6) and (8), the seepage flow of the tunnel is given by

$$Q=\frac{2\pi k_1k_2(H_w-h_1)}{k_1\ln\left[\frac{H}{r_2}-\sqrt{\left(\frac{H}{r_2}\right)^2-1}\right]+k_2\ln\frac{r_2}{r_1}} \tag{9}$$

The hydraulic head h_2 and the water pressure P at the outer edge of the tunnel lining are as follows

$$h_2=\frac{\ln\frac{r_2}{r_1}H_w+\frac{k_1}{k_2}h_1\ln\left[\frac{H}{r_2}-\sqrt{\left(\frac{H}{r_2}\right)^2-1}\right]}{\frac{k_1}{k_2}\ln\left[\frac{H}{r_2}-\sqrt{\left(\frac{H}{r_2}\right)^2-1}\right]+\ln\frac{r_2}{r_1}} \tag{10}$$

$$P=\gamma_w h_2=\gamma_w\frac{\ln\frac{r_2}{r_1}H_w+\frac{k_1}{k_2}h_1\ln\left[\frac{H}{r_2}-\sqrt{\left(\frac{H}{r_2}\right)^2-1}\right]}{\frac{k_1}{k_2}\ln\left[\frac{H}{r_2}-\sqrt{\left(\frac{H}{r_2}\right)^2-1}\right]+\ln\frac{r_2}{r_1}} \tag{11}$$

The extraction of common factors allows for the establishment of a correlation between the tunnel inflow Q and the lining water pressure P

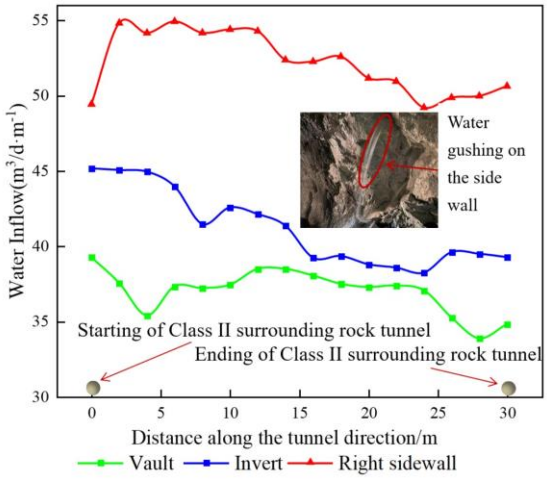

Fig. 4 Monitoring curve of class II tunnel water inflow

$$Q=\frac{2\pi k_1}{\ln\frac{r_2}{r_1}+2\pi k_1 h_1}\times\frac{1}{\gamma_w}\times P \tag{12}$$

The formula addresses the issue of relatively constant parameters in current tunnel inflow prediction by converting tunnel depth, seawater depth, and other parameters into dynamic variables such as water pressure and lining inner wall hydraulic head. The formula can provide more accurate predictions of water inflow based on the water pressure at different locations.

According to formula (12), the water inflow at different points in the tunnel is positively correlated with the pore water pressure behind the lining. As illustrated in the figure, the maximum water inflow in the class II surrounding rock tunnel of sea section occurs at the right sidewall, reaching approximately 55 m³/(d·m). Comparisons with on-site water inflow data indicate that during actual construction, the water inflow at the tunnel right sidewall is generally greater than at other locations.

4. Establishment of three-dimensional numerical models for different sections of subsea tunnel

4.1 Model establishment

To simplify the calculations and take into account the characteristics of the rock formations in both the land and sea sections of the Shantou. The model was established using Rhino (6.9) and imported into FLAC 3D (6.0) software for numerical simulation calculations. The surrounding rock within a range of 5 times the tunnel diameter is selected as the analysis object. The coordinate system is established with the vertical axis (Z-axis) representing the vertical direction, the tunnel axis (Y-axis) representing the direction along the tunnel axis, and the vertical tunnel axial (X-axis) representing the lateral direction. Three-dimensional simulation models are created to numerically simulate and calculate the tunnel and surrounding rock in three sections: the land section, the transition section between land and sea, and the sea section. The model setup is shown in Figs. 5-7.

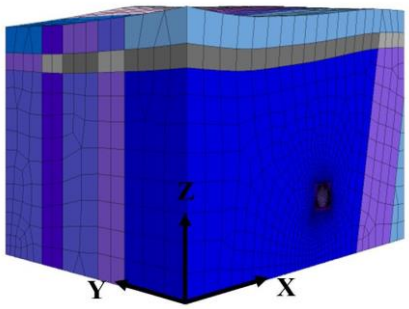

Fig. 5 Numerical model of land section

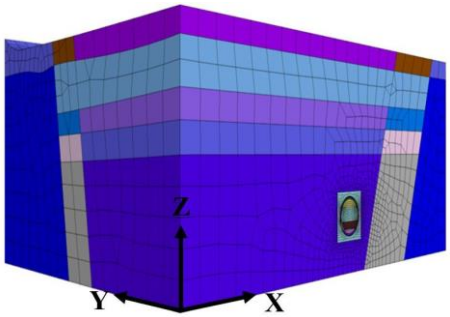

Fig. 6 Numerical model of sea section

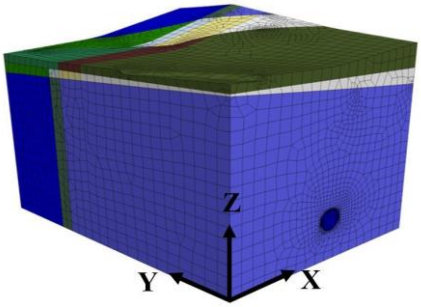

Fig. 7 Numerical model of transition section between land and sea

Based on field stress testing and engineering experience, the boundary conditions are set with normal displacement constraints applied to the four sides and the bottom, while the top surface is left unconstrained.

4.2 Parameter selection

The excavation and support procedures in the model are completely consistent with the on-site construction methods. For the IV and V rock mass classifications, a three-step excavation method is employed, while the II rock mass classification is excavated using a full-section excavation method. The lining material is C30 concrete, lining is simulated using the entity unit, support is simulated using the "cable" and "liner" elements in the FLAC program. The waterproof material is waterproof coil. In the simulation process, the waterproof simulation is realized by setting the unit as impervious unit. The overall model adopts the Mohr-Coulomb constitutive model, which is suitable for isotropic granite materials. The physical and mechanical parameters of the rock mass are listed in Table 1.

Table 1 Physical and mechanical parameters of the rock mass

Rock Type	Elastic Modulus/GPa	Density/ (kg/m^3)	Poisson's Ratio	Cohesion /MPa	Internal Friction Angle /(°)	Tensile Strength /MPa
Granite (Class II Rock)	83.0	2670	0.2	13.3	49	120
Granite (Class III Rock)	66.4	2436	0.25	10.7	40	100
Granite (Class IV Rock)	5.31	1949	0.31	8.48	32	80
Granite (Class V Rock)	3.72	1364	0.39	5.94	22	50

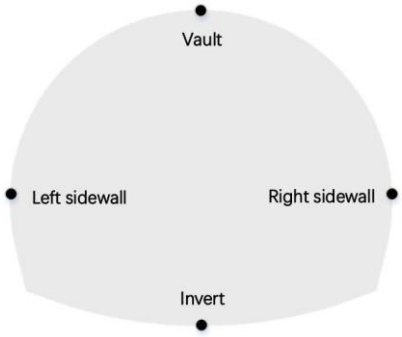

Fig. 8 Layout of monitoring points for three concentric circular cross-sections

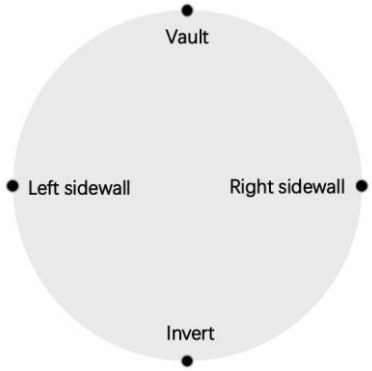

Fig. 9 Layout of monitoring points for circular cross-sections

4.3 Layout of monitoring points

Monitoring points are arranged along the tunnel axis with the initial excavation face as the origin, with a spacing of 2 meters between each point. The layout of monitoring points for three concentric circles and circular cross-sections is shown in Figs. 8 and 9. Due to the symmetry of the tunnel cross-section, monitoring is conducted on either the left or right set of points.

5. Study on optimal waterproofing and drainage solutions for different sections of the tunnel

5.1 Analysis of land section calculation results

The land section of the tunnel passes through the IV-class and II-class rock mass sections. A comparative analysis is conducted to analyze the displacement and pore water pressure of the tunnel under different waterproofing and drainage systems for these two rock mass classes, in order to determine an appropriate waterproofing and drainage solution.

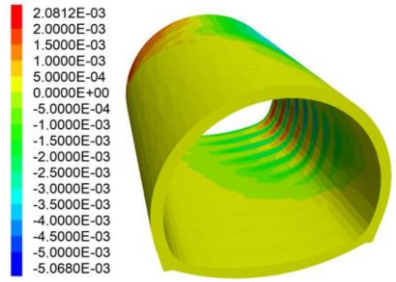

(a) Full encapsulated waterproofing system

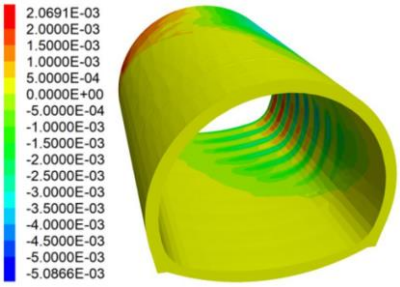

(b) Half encapsulated waterproofing system

Fig. 10 Displacement field of land section IV-class rock mass tunnel lining structure in the X direction

5.1.1 Deformation analysis of tunnel lining structure

The displacement distribution diagrams of the X and Z directions of the land section IV-class rock mass for the tunnel lining structure are shown in Figs. 10 and 11. The overall distribution of displacement field is relatively similar between the full encapsulated and half encapsulated waterproofing systems. However, due to the influence of a fault zone in the latter half of the tunnel, the internal structure of the IV-class rock mass tunnel lining exhibits significant phased variations, resulting in larger displacements in the latter half of the tunnel. In the sections where no fault zone is present, the horizontal and vertical displacements of the tunnel remain relatively stable.

Monitoring was conducted at various positions along the axial lining structure of the tunnel, and the curves are shown in Fig. 12.

Based on Fig. 12, it can be observed that there is little difference in the X-direction displacements between the full encapsulated and half encapsulated waterproofing systems.

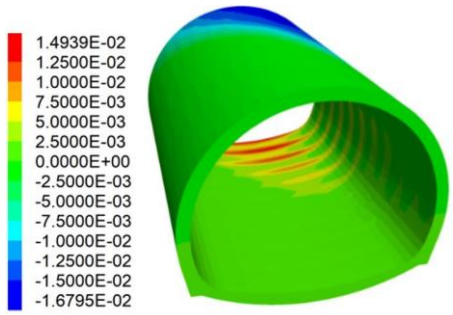

(a) Full encapsulated waterproofing system

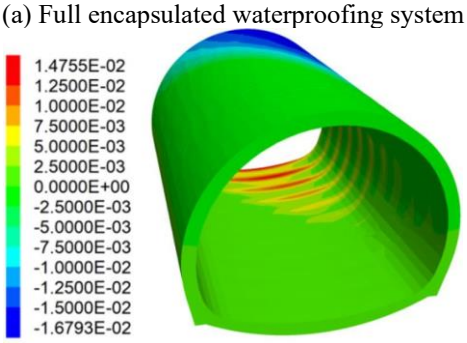

(b) Half encapsulated waterproofing system

Fig. 11 Displacement field of land section IV-class rock mass tunnel lining structure in the Z direction

The maximum incremental displacement is approximately 2 mm for the right sidewall, indicating that the overall displacement variation of the tunnel is within the safe deformation range of the lining. Additionally, due to unfavorable geological conditions in the land section IV-class rock mass, the displacement variations of the vault and invert increase progressively with the advancement of monitoring points. The maximum displacement deformation at the vault is 6 mm, while at the invert it is 8 mm. Therefore, special attention should be given to vault collapse and invert uplift during construction.

The displacement distribution diagrams of the land section II-class rock mass in the X-direction and Z-direction of the lining structure are shown in Figs. 13 and 14, respectively.

Based on Figs. 13 and 14, it can be observed that there is little significant phased variation in the internal lining structure of the land section II-class rock mass tunnel under both full encapsulated and half encapsulated waterproofing systems. In the X-direction displacement field, the displacements at the invert exhibits a distinct symmetric distribution. In the Z-direction displacement field, the overall displacement variations at the invert are smaller in the half encapsulated waterproofing system compared to the full encapsulated waterproofing system. Due to the sudden increase or decrease in the exposed face area of the tunnel, certain excavation disturbances occur. As a result, significant settlements occur at the invert of both full encapsulated and half encapsulated waterproofing systems at the transition sections between tunnels with different rock mass levels. Monitoring curves for various positions of the lining structure in the land section II-class rock mass tunnel are shown in Fig. 15.

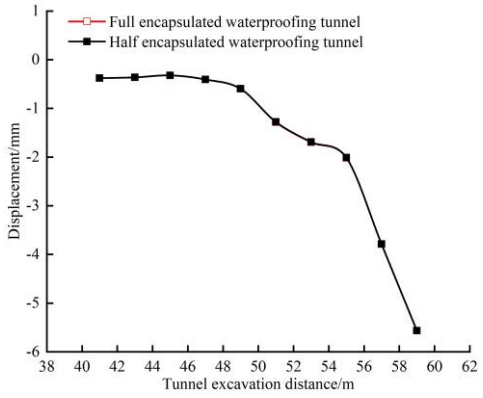

(a) Monitoring point for vault displacement

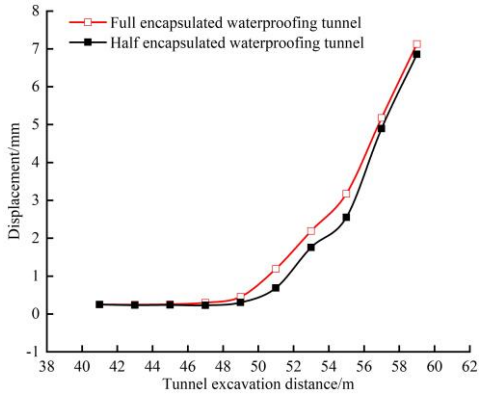

(b) Monitoring point for invert displacement

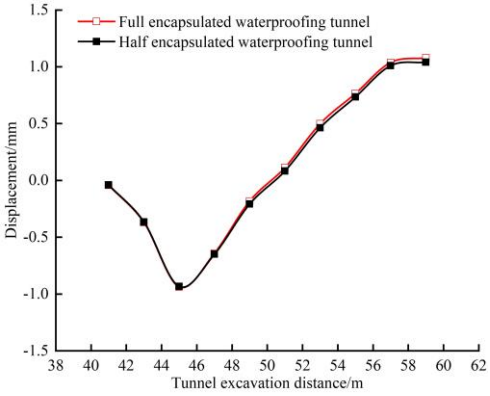

(c) Monitoring point for right sidewall displacement

Fig. 12 Monitoring curves of lining deformation in the land section IV-class rock mass

From Fig. 15, it can be observed that the overall deformation of the tunnel lining structure is relatively small. The overall displacement change of the tunnel is stable, and the displacement variation is within the safe deformation range of the lining. The difference in displacement at the vault under the two waterproofing systems can also be neglected, with a maximum displacement of approximately 1mm. The deformation of the lining structure mainly concentrates in the vertical direction of the vault. Therefore, it is important to monitor the displacement variation at this location and ensure real-time protection during construction.

5.1.2 Tunnel lining pore water pressure analysis

Under both full encapsulated and half encapsulated

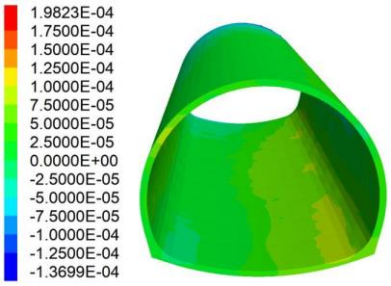

(a) Full encapsulated waterproofing system

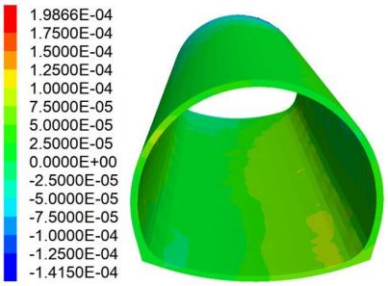

(b) Half encapsulated waterproofing system

Fig. 13 Displacement field of land section II-class rock mass tunnel lining structure in the X direction

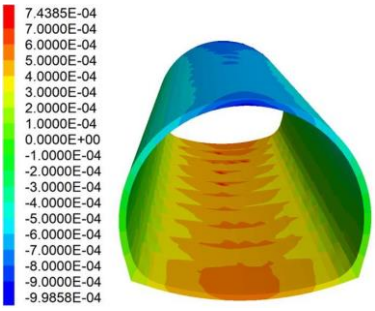

(a) Full encapsulated waterproofing system

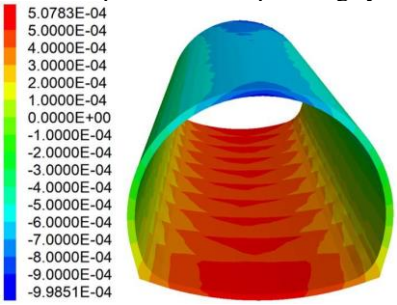

(b) Half encapsulated waterproofing system

Fig. 14 Displacement field of land section II-class rock mass tunnel lining structure in the Z direction

waterproofing systems in the terrestrial IV-class rock mass tunnel, the pore water pressure at the sidewalls is significantly higher than that at the outer side of the vault. In the half encapsulated waterproofing system, the distribution of pore water pressure at the bottom of the invert is uneven, and there is a concentrated area of pore water pressure at the junction of the side walls and the invert. This phenomenon is most pronounced in rock masses of lower quality. The pore water pressure distribution behind the lining of the land section IV-class rock mass tunnel is shown in Fig. 16.

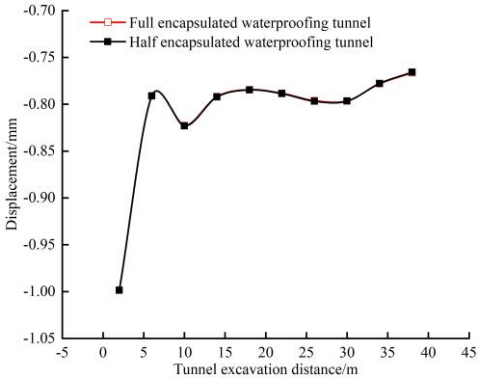

(a) Monitoring point for vault displacement

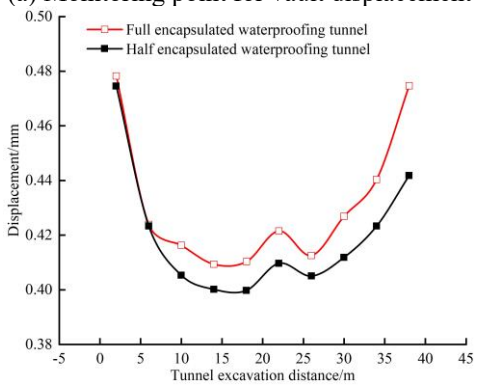

(b) Monitoring point for invert displacement

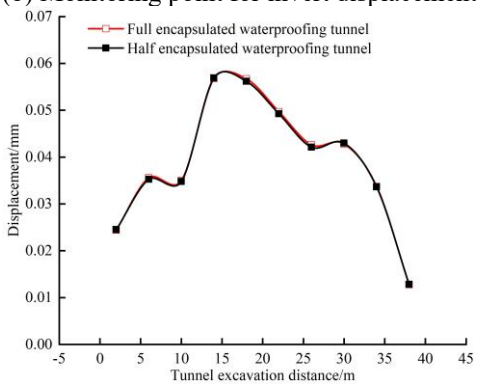

(c) Monitoring point for right sidewall displacement

Fig. 15 Monitoring curves of lining deformation in land section II-class rock mass

Fig. 17 shows the monitoring curve of pore water pressure at different positions of the lining structure.

According to the analysis from Fig. 17, it can be observed that under the comparison of full encapsulated and half encapsulated waterproofing systems, the trend of pore water pressure variation is basically the same. The pore water pressure gradually increases at the invert and vault, with an overall increment of approximately 0.6 MPa. This increase can be attributed to the decrease in mechanical properties of the rock mass at the second half of the tunnel that crosses the fault zone, resulting in an increase in pore water pressure at the corresponding locations. The variation in pore water pressure at the sidewalls is relatively small and stable. The pore water pressure distribution behind the lining of the land section II-class rock mass tunnel is shown in Fig. 18.

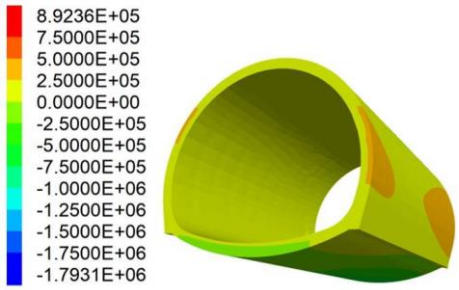

(a) Full encapsulated waterproofing system

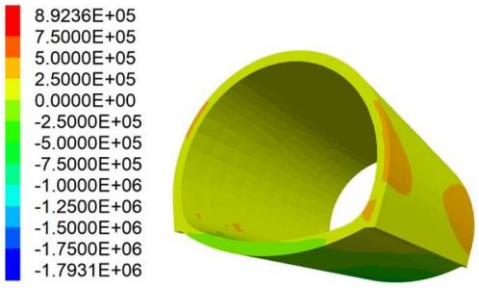

(b) Half encapsulated waterproofing system

Fig. 16 Pore water pressure distribution diagrams of land section class IV rock mass

From Fig. 18, it can be observed that in the land section II-class rock mass tunnel, under both full encapsulated and half encapsulated waterproofing systems, the pore water pressure is generally distributed evenly. The pore water pressure at the left and right walls is significantly greater than that at the outer side of the vault. In the case of the half encapsulated waterproofing system, the distribution of pore water pressure at the bottom of the II-class rock mass invert is uneven, with a concentrated area of pore water pressure at the junction of the sidewalls and invert. Monitoring of pore water pressure at various locations of the lining structure is depicted by the curves in Fig. 19.

From Fig. 19, it can be seen that under both full encapsulated and half encapsulated waterproofing systems, the pore water pressure at the sidewalls gradually increases, with an increment of approximately 0.08 MPa. Although the pore water pressure at the vault and invert fluctuates in a serrated pattern, the fluctuation amplitude is small and gradually increases. The pore water pressure at the vault is concentrated between 0.5 MPa and 0.6 MPa, which is generally higher than the pore water pressure at the invert.

Taking everything into consideration, there is little difference in pore water pressure between the full encapsulated and half encapsulated waterproofing systems in the tunnel. Both systems exhibit concentrated pore water pressure at the junction of the sidewalls and invert. However, the overall deformation of the tunnel under the half encapsulated waterproofing system is smaller than those under the full encapsulated system. Additionally, the half encapsulated waterproofing system requires significantly fewer waterproofing materials compared to the full encapsulated waterproofing system. Therefore, from an economic standpoint aiming to save materials, the half encapsulated waterproofing system is prioritized for the land section in subsea tunnels.

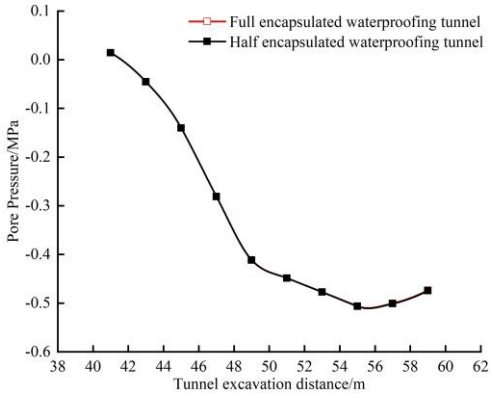

(a) Monitoring point for pore water pressure at the vault

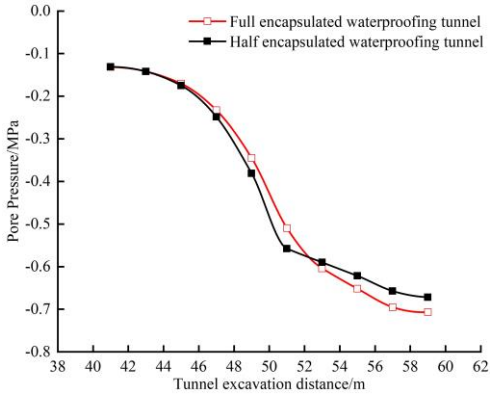

(b) Monitoring point for pore water pressure at the invert

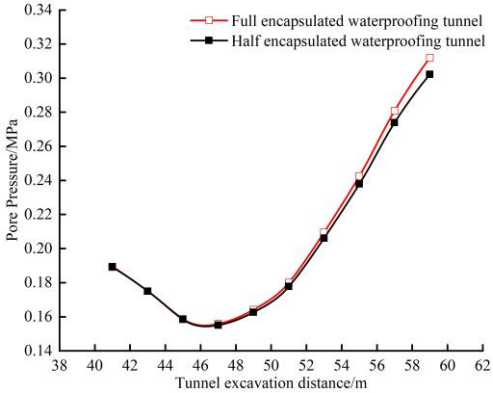

(c) Monitoring point for pore water pressure at the right sidewall

Fig. 17 Monitoring curves of pore water pressure in the lining of land section IV-class rock mass

5.2 Analysis of sea section calculation results

The sea section of the tunnel traverses through class V, class IV, and class II surrounding rocks. The subsea tunnel has a large burial depth and exhibits a “V” shape, with a lower middle section and higher sides. Drainage inside the tunnel is inconvenient, and utilizing a half encapsulated waterproofing system would require a large number of pumping equipment and manpower resources, resulting in unnecessary economic waste. Therefore, only a full encapsulated waterproofing system design is considered, analyzing the stability of the tunnel under the full encapsulated waterproofing system.

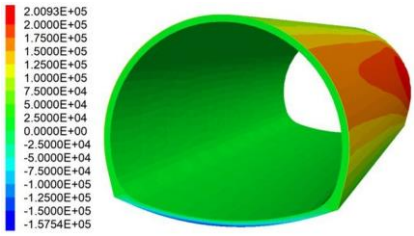

(a) Full encapsulated waterproofing system

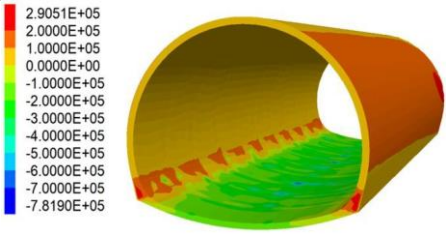

(b) Half encapsulated waterproofing system

Fig. 18 Pore water pressure distribution diagrams of land section class II rock mass

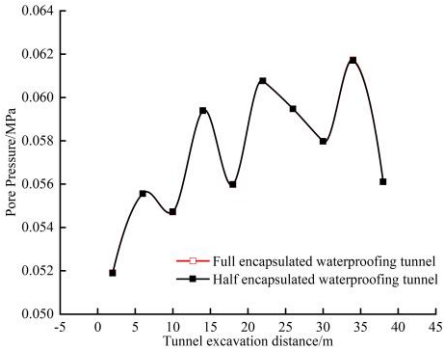

(a) Monitoring point for pore water pressure at the vault

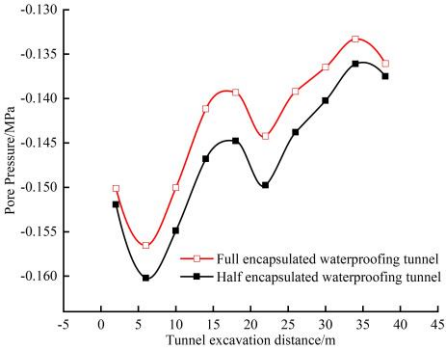

(b) Monitoring point for pore water pressure at the invert

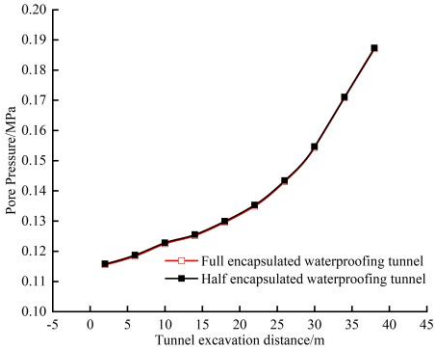

(c) Monitoring point for pore water pressure at the right sidewall

Fig. 19 Monitoring curves of pore water pressure in the lining of land section II-class rock mass

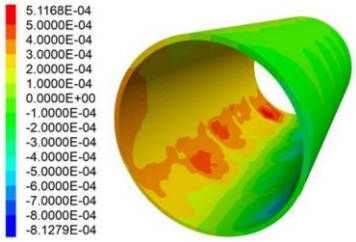

(a) Sea section class II rock mass

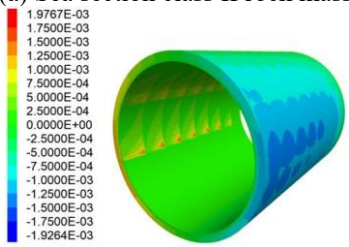

(b) Sea section class IV rock mass

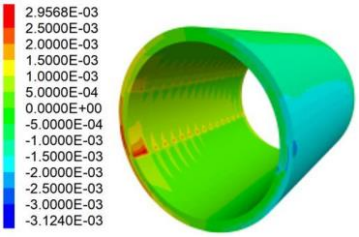

(c) Sea section class V rock mass

Fig. 20 X-direction deformation distribution diagrams of sea section lining structure

5.2.1 Deformation analysis of tunnel lining structure

The deformation of the surrounding rocks in the sea section of the tunnel mainly manifests as deformation towards the center from the left and right sidewalls, as well as downward deformation of the vault and upward deformation of the invert. Horizontal displacement field distribution diagrams for various classes of surrounding rocks in the subsea tunnel are shown in Fig. 20.

According to Fig. 20, in the X-direction displacement field, the deformation of the tunnel lining exhibits a symmetrical distribution with the tunnel center's Z-axis as the axis of symmetry, showing an overall trend of convergence towards the tunnel center. As the class of the surrounding rocks increases, with a decrease in rock quality, the deformation of the class V surrounding rock tunnel is significantly larger than that of the class II surrounding rock tunnel. Both class IV and class V tunnels are excavated using a stepped excavation method, and multiple excavations can cause multiple disturbances at the junction of upper, middle, and lower steps. Therefore, there is a noticeable increase in horizontal displacement at the step junctions, and it is necessary to monitor the structural deformation at these locations during construction. Extracted Z-direction displacement distribution diagrams for various classes of surrounding rocks in the subsea tunnel are shown in Fig. 21.

In the Z-direction displacement field, the deformation of the tunnel lining in the surrounding rocks exhibits a symmetrical distribution with the tunnel center's X-axis as the axis of symmetry, showing an overall trend of vault

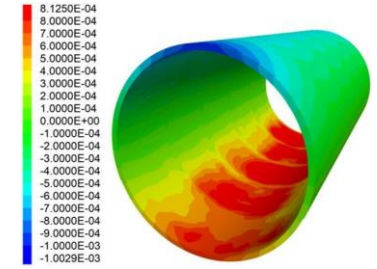

(a) Sea section class II

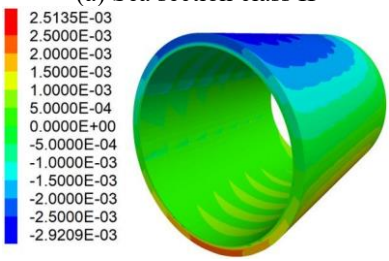

(b) Sea section class IV

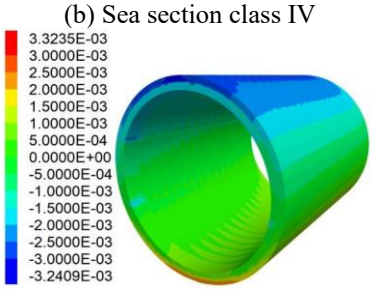

(c) Sea section class V

Fig. 21 Z-direction deformation distribution diagrams of sea section lining structure

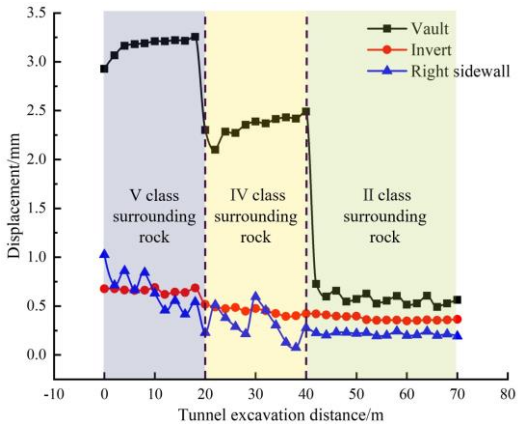

Fig. 22 Monitoring curves of deformation in sea section lining

subsidence and invert uplift. The deformation of the class V surrounding rock tunnel is significantly larger than that of the class II surrounding rock tunnel. Due to the poor stability of the rock at the boundary between different rock classes, there is a noticeable increase in deformation at the invert of the tunnel in front of both class IV and class V tunnels. During construction, it may be possible to reduce the abrupt deformation at this location by implementing a transitional section using different construction methods. Extracted monitoring curves for the deformation of the lining structure are shown in Fig. 22.

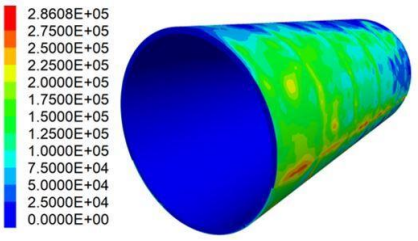

(a) Sea section class II rock mass

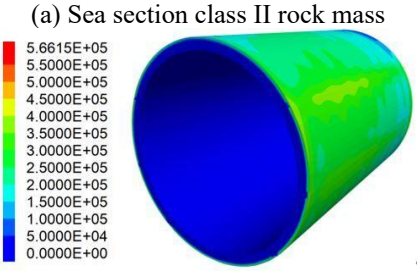

(b) Sea section class IV rock mass

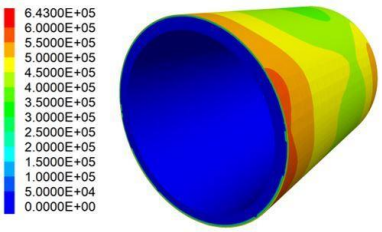

(c) Sea section class V rock mass

Fig. 23 Pore water pressure distribution diagrams of sea section

According to Fig. 22, the deformation of the three monitoring points exhibits regional variations, with better rock classes resulting in smaller deformations of the lining structure after excavation. As the tunnel progresses from class V (20 m) to class IV (20 m) and further to class II (30 m), the overall deformation of the tunnel significantly decreases. Looking at the displacement of the vault, the deformation in the class V rock tunnel is approximately 1.23 times that in class IV tunnel and approximately 6.2 times that of the class II tunnel. The maximum deformation in the class V rock tunnel is around 3.2 mm, in the class IV rock tunnel it is around 2.6 mm, and in the class II rock tunnel it is around 0.5 mm. All these maximum deformations occur at the vault. Therefore, special attention should be given to monitoring the settlement of the vault during construction in order to take timely reinforcement measures.

5.2.2 Tunnel lining pore water pressure analysis

Based on the distribution diagrams of pore water pressure, it can be observed that the pore water pressure is mainly distributed in the upper part of the lining structure (vault and sidewalls). Significant pore water pressure can also occur at the boundary between different rock classes. Extracted pore water pressure distribution diagrams for various rock classes in the subsea tunnel are shown in Fig. 23.

From Fig. 23, it can be observed that the maximum pore water pressure in the class II rock tunnel is primarily distributed at the invert and at the junction between the

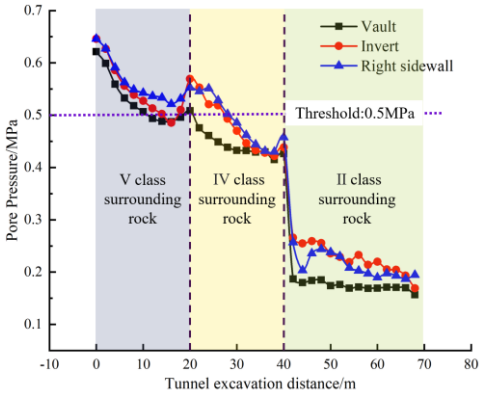

Fig. 24 Monitoring curve of pore water pressure behind the lining in the sea section

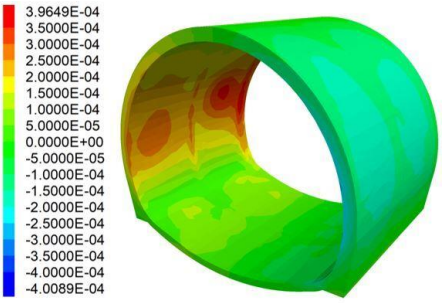

(a) Land section III class

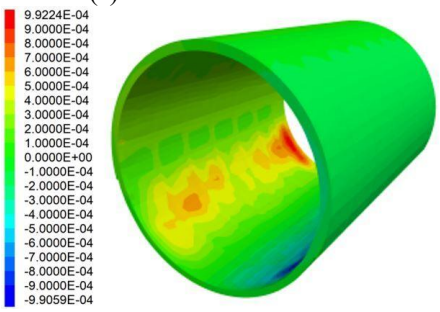

(b) Sea section III class

Fig. 25 Displacement field of lining structure in the X-direction in transition section between land and sea

sidewalls and the invert. In the class IV rock tunnel, areas with high pore water pressure are mainly located at the back of the invert lining and at the anterior and posterior cross-sections of the tunnel as a whole. In the class V rock tunnel, areas with high pore water pressure are mainly distributed at the anterior and posterior cross-sections of the tunnel. In subsea tunnels with poorer rock classes, higher pore water pressure is likely to occur when crossing the boundaries between different rock classes. Additionally, as the rock class deteriorates, the tunnel becomes more permeable and water flow channels within the rock mass increase, resulting in higher pore water pressure behind the lining. The extracted pore water pressure behind the lining is shown in Fig. 24.

From Fig. 24, it can be observed that as the tunnel progresses from class V (20 m) excavation to class IV (20 m) and then to class II (30 m), the better the rock quality, the lower the pore water pressure behind the lining after excavation. In particular, the vertical displacement at the

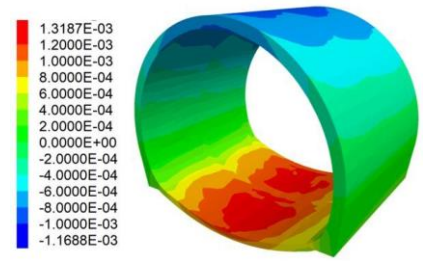

(a) Land section III class

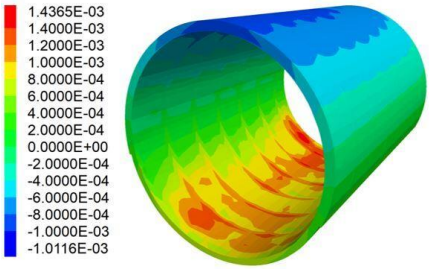

(b) Sea section III class

Fig. 26 Displacement field of lining structure in the Z-direction in transition section between land and sea

tunnel's vault in the class V rock tunnel is approximately 1.18 times that of the class IV tunnel and about 2.75 times that of the class II tunnel. The hydraulic head at the invert is high resulting in the maximum pore water pressure occurring at the invert. The maximum pore water pressure behind the lining in the class V tunnel is around 0.65 MPa, in the class IV tunnel it is around 0.56 MPa, and in the class II tunnel it is around 0.23 MPa. Therefore, it is important to monitor the pore water pressure at the invert during construction.

Overall, only certain sections of the class V and class IV tunnels have pore water pressures exceeding 0.5 MPa, and the pore water pressure in the invert is generally higher than that at the vault. Considering the actual situation, adopting a full encapsulated waterproofing system is a more suitable choice. Due to the impermeable nature and fully sealed structure of the subsea tunnel with a full encapsulated waterproofing system, there will be relatively high pore water pressure on the lining surface. Therefore, while choosing a full encapsulated waterproofing system, controlled drainage should be implemented. This can be achieved by installing pressure relief valves at locations with high water pressure and discharging water when the pressure exceeds the threshold. Additionally, reinforcement of the weak sections of the tunnel should be strengthened.

5.3 Analysis of transition section between land and sea calculation results

The transition section between land and sea tunnels traverses class III rock sections in both land and sea areas. Based on the previous research results, a half encapsulated waterproofing system is used in the land section, while a full encapsulated waterproofing system is used in the sea section. A comparative analysis of the displacement field and pore water pressure in this research section is conducted to analyze the deformation characteristics of the

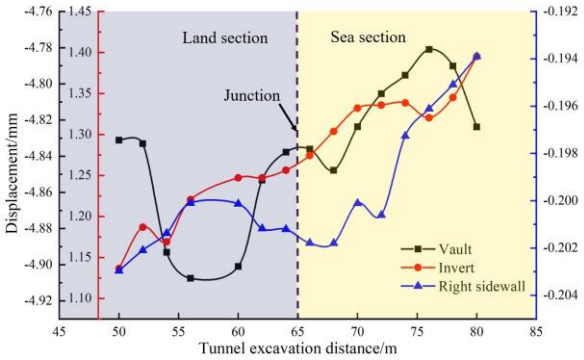

Fig. 27 Monitoring curves of lining deformation in transition section between land and sea

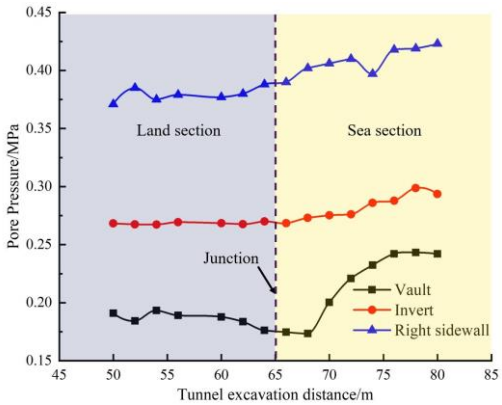

Fig. 28 Monitoring curves of pore water pressure behind the lining in transition section between land and sea

tunnel lining structure and the distribution patterns of pore water pressure behind the lining.

5.3.1 Tunnel lining structure deformation analysis

The deformation of the surrounding rock in the transition section between land and sea tunnels is mainly characterized by deformation towards the center from the sidewalls and downward deformation of the vault with upward deformation of the invert. The extracted horizontal displacement field distribution diagrams for various rock classes are shown in Fig. 25.

Based on Fig. 25, it can be observed that in the horizontal displacement field, the deformation of the tunnel lining is symmetrically distributed with the tunnel center's Z-axis as the axis of symmetry. It generally shows a tendency to converge towards the center of the tunnel. Additionally, the sea section experiences larger deformations compared to the land section. The vertical displacement field of the subsea tunnel for various rock mass ratings is depicted in Fig. 26.

Based on Fig. 26, it can be observed that in the vertical displacement field, the deformation of the tunnel lining is symmetrically distributed with the tunnel center's X-axis as the axis of symmetry. It generally shows a tendency to converge towards the center of the tunnel. Additionally, the sea section experiences slightly larger deformations compared to the land section, with the maximum deformations occurring at the position of the vault. The extracted deformation values of the lining structure are shown in Fig. 27.

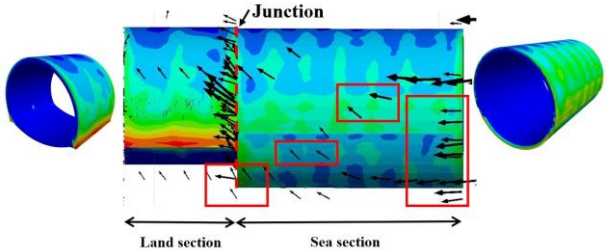

Fig. 29 Distribution of pore water pressure and water flow direction in transition section between land and sea

From Fig. 27, it can be observed that during the excavation process from the III class surrounding rock in the land section to the III class surrounding rock in the sea section, there is overall fluctuation in the deformation of the surrounding rock. The settlement at the vault fluctuates within the range of 0.78 to 0.92 mm, the heave at the invert fluctuates within the range of 1.15 to 1.40 mm, and the deformation of the sidewalls fluctuates within the range of 0.19 to 0.2 mm. Therefore, the transition between the land section and the sea section using different construction methods does not have a significant impact on the deformation of the surrounding rock for the same rock class.

5.3.2 Tunnel lining pore water pressure analysis

Monitoring of the pore water pressure on the tunnel lining in the transition section between the land and sea sections was conducted, and the monitoring curves are shown in Fig. 28. By examining the variation curve of pore water pressure, it is evident that there is a significant increase in pore water pressure behind the lining after 65 m (at the interface between the land and the sea section). The pore water pressure at the invert increases from 0.265 MPa to 0.3 MPa, at the vault from 0.18 MPa to 0.24 MPa, and at the sidewalls from 0.39 MPa to 0.42 MPa. Therefore, special attention should be paid to the variation of pore water pressure at this interface during construction to promptly address potential sudden water inflow situations.

The distribution of pore water pressure and water flow direction in the transition section between land and sea tunnels is shown in Fig. 29. The variation pattern of pore water pressure at the vault is generally consistent between the full encapsulated waterproofing and half encapsulated waterproofing systems. In the land section, significant pore water pressure occurs at the interface between the sidewalls and the invert. It is important to monitor the stability of the surrounding rock at that location during construction.

In the transition section between land and sea tunnels, the law in the land section follows the general trend of land sections, while the law in the sea section follows the general trend of sea sections. Due to the different characteristics of the half encapsulated waterproofing and full encapsulated waterproofing systems, significant pore water pressure can occur at the interface between the land section and the sea section. The water flow tends to flow from the sea section of high pore water pressure to the invert position of the half

encapsulated waterproofing section of the land section. During construction, special attention should be given to the hydraulic head difference between the full encapsulated waterproofing and half encapsulated waterproofing systems at the interface. Adequate measures should be taken for waterproofing and drainage in the half encapsulated waterproofing structures of the land section.

6. Conclusions

Based on the theoretical framework of complex variable functions and Darcy's law, this study proposes a dynamic parameter-based formula for predicting water inflow in subsea tunnels. The formula integrates tunnel depth, hydraulic head, and lining permeability, providing a more adaptable approach compared to traditional static parameter models. This advancement offers a reliable tool for estimating water inflow under varying hydraulic conditions.

In the land section, the half-encapsulated waterproofing system demonstrated smaller overall deformation (15-20% reduction) compared to the fully encapsulated system, with minimal differences in pore water pressure. The reduced material usage and cost-effectiveness of the half-encapsulated system make it the preferred choice for this section.

In the sea section, pore water pressure generally remained below 0.5 MPa, except in localized zones with class IV and V rock masses. Due to the challenges of on-site drainage, a fully encapsulated waterproofing system is recommended. Pressure-relief valves should be installed in high-pressure areas to manage water pressure effectively, and weak sections should be reinforced to ensure structural stability.

The transition section between the land and sea segments exhibited elevated pore water pressure (up to 0.42 MPa) at the interface, driven by hydraulic head differentials between the fully encapsulated and half-encapsulated systems. Adaptive drainage measures are essential in this area to mitigate seepage risks and ensure smooth transitions between waterproofing systems.

While the analytical formula for water inflow prediction and the numerical simulations for stability analysis address distinct aspects of subsea tunnel design, their combined insights provide a comprehensive framework for optimizing waterproofing-drainage systems. This integrated approach enhances the safety, stability, and cost-effectiveness of subsea tunnels.

Acknowledgements

The authors gratefully acknowledge Shandong Jianzhu University, Shandong University and Shandong University of Science and Technology that have contributed to the research results reported within this paper. This study was financially supported by the National Natural Science Foundation of China (No.42172310), the Youth Innovation Project of Science and Technology of University in Shandong Province (2019KJG015) and supported by the TaiShan Scholars Program (No.tsqn202408226, No.tsqn202312192).

References

Aalianvari, A. (2017), "Combination of engineering geological data and numerical modeling results to classify the tunnel route based on the groundwater Seepage", *Geomech. Eng.*, **13**(4), 671-683. https://doi.org/10.12989/gae.2017.13.4.671.

Arjnoi, P., Jeong, J.H., Kim, C.Y. and Park, K.H. (2009), "Effect of drainage conditions on pore water pressure distributions and lining stresses in drained tunnels", *Tunn. Undergr. Sp. Tech.*, **24**(4), 376-389. https://doi.org/10.1016/j.tust.2008.10.006.

Butscher, C. (2012), "Steady-state groundwater inflow into a circular tunnel", *Tunn. Undergr. Sp. Tech.*, **32**, 158-167. https://doi.org/10.1016/j.tust.2012.06.007.

Dammyr, O., Nilsen, B., Thuro, K. and Grondal, J. (2014), "Possible concepts for waterproofing of Norwegian TBM railway tunnels", *Rock Mech. Rock Eng.*, **47**(3), 985-1002. https://doi.org/10.1007/s00603-013-0388-5.

Farhadian, H. and Nikvar-Hassani, A. (2019), "Water flow into tunnels in discontinuous rock: A short critical review of the analytical solution of the art", *Bull. Eng. Geol. Environ.*, **78**(5), 3833-3849. https://doi.org/10.1007/s10064-018-1348-9.

Golian, M., Teshnizi, E.S. and Nakhaei, M. (2018), "Prediction of water inflow to mechanized tunnels during tunnel-boring-machine advance using numerical simulation", *Hydrogeol. J.*, **26**(8), 2827-2851. https://doi.org/10.1007/s10040-018-1835-x.

Huang, F., Tan, Z., Wang, M. and Wang, X. (2009), "Analytical solutions for water in flow into an underwater tunnel and its application", *Strategic Study of CAE*, **11**(7), 66-70.

Kolymbas, D. and Wagner, P. (2007), "Groundwater ingress to tunnels: The exact analytical solution", *Tunn. Undergr. Sp. Tech.*, **22**(1), 23-27. https://doi.org/10.1016/j.tust.2006.02.001.

Li, C., Hu, Y., Ding, J., Wu, F. and Zhen, B. (2012), "Research on design theory and methodology for tunnel groundwater treatment", *J. Eng. Geol.*, **20**(5), 832-840.

Li, P.F., Feng, C.H., Liu, H.C., Zhao, Y., Li, Z. and Xiong, H.C. (2021), "Development and assessment of a water pressure reduction system for lining invert of underwater tunnels", *Mar. Georesour. Geotech.*, **39**(3), 365-371. https://doi.org/10.1080/1064119X.2019.1703126.

Li, S.C., He, P., Li, L.P., Shi, S.S., Zhang, Q.Q., Zhang, J. and Hu, J. (2017), "Gaussian process model of water inflow prediction in tunnel construction and its engineering applications", *Tunn. Undergr. Sp. Tech.*, **69**, 155-161. https://doi.org/10.1016/j.tust.2017.06.018.

LI, Z., He, C., Ding, J. and Yang, S. (2017), "A prediction method for the relationship between displacement and water pressure in urban tunnel operation period", *Eng. Mech.*, **34**(1), 14-21. https://doi.org/10.6052/j.issn.1000-4750.2015.05.0419.

Ming, H.F., Wang, M.S., Tan, Z.S. and Wang, X.Y. (2010), "Analytical solutions for steady seepage into an underwater circular tunnel", *Tunn. Undergr. Sp. Tech.*, **25**(4), 391-396. https://doi.org/10.1016/j.tust.2010.02.002.

Nilsen, B. (2014), "Characteristics of water ingress in Norwegian subsea tunnels", *Rock Mech. Rock Eng.,* **47**(3), 933-945. https://doi.org/10.1007/s00603-012-0300-8.

Pan, Y.H., Qi, J.R., Zhang, J.F., Peng, Y.X., Chen, C., Ma, H.N. and Ye, C. (2022), "A comparative study on steady-state water inflow into a circular underwater tunnel with an excavation damage zone", *Water*, **14**(19). https://doi.org/10.3390/w14193154.

Pan, Y. (2004), Complex Variables Function, Science Press, Beijing, China.

Park, K.H., Adisorn, O. and Lee, J.G. (2008), "Analytical solution for steady-state groundwater inflow into a drained circular tunnel in a semi-infinite aquifer: A revisit", *Tunn. Undergr. Sp. Tech.*, **23**(2), 206-209. https://doi.org/10.1016/j.tust.2007.02.004.

Shin, J.H., Choi, K.C., Yoon, J.U. and Shin, Y.J. (2011), "Hydraulic significance of fractured zones in subsea tunnels", *Mar. Georesour. Geotec.*, **29**(3), 230-247. https://doi.org/10.1080/1064119X.2011.555712.

Wang, X., Tan, Z., Li, J. and Du, C. (2012), "Laboratory tests on mechanical characteristics of fully and partially wrapped waterproof systems for tunnel lining", *Chinese J. Geotech. Eng.*, **34**(4), 654-659.

Wang, X., Tan, Z., Wang, M., Liang, W. and Zhang, M. (2007), "Study on waterproof and drainage principles of Xiamen", *Chinese J. Rock Mech. Eng.*, **193**(2), 3810-3815.

Wang, X., Wang, M., Zhang, M. and Ming, H. (2008), "Theoretical and experimental study of external water pressure on tunnel lining in controlled drainage under high water level", *Tunn. Undergr. Sp. Tech.*, **23**(5), 552-560. https://doi.org/10.1016/j.tust.2007.10.004.

Ying, H.W., Zhu, C.W.; Shen, H.W. and Gong, X.N. (2018), "Semi-analytical solution for groundwater ingress into lined tunnel", *Tunn. Undergr. Sp. Tech.*, **76**, 43-46. https://doi.org/10.1016/j.tust.2018.03.009.

Zareifard, M.R. (2018), "An analytical solution for design of pressure tunnels considering seepage loads", *Appl. Math. Model.*, **62**, 62-85. https://doi.org/10.1016/j.apm.2018.05.032.

Zhang, D. and Sun, Z. (2019), "Active control system for underwater tunnel and its design method", *Chinese J. Rock Mech. Eng.*, **38**(1), 1-17. https://doi.org/10.13722/j.cnki.jrme.2018.0955.

Zhang, L.W., Zhao, D.K., Wu, J., Yang, W.M., Wang, W. and Xin, D.D. (2020), "Prediction of water inflow in Tsingtao subsea tunnel based on the superposition principle", *Tunn. Undergr. Sp. Tech.*, **97**, 1-12. https://doi.org/10.1016/j.tust.2019.103243.

Zhang, Y., Liu, Z. and Sun, X. (2022), "Research on physical field distribution law of different water proof and drainage forms in high water pressure submarine tunnel", *Traffic Eng. Tech. Nat. Defence*, **20**(2), 29-32+80. https://doi.org/10.13219/j.gjgyat.2022.02.007.

Zhu, C., Ying, H., Gong, X., Shen, H. and Wang, X. (2019), "Analytical study on seepage field of underwater parallel tunnel", *Chinese J. Geotech. Eng.*, **41**(2), 355-360. https://doi.org/10.11779/CJGE201902014.

Zou, J.F., Wei, A. and Liang, L. (2020), "Analytical solution for steady seepage and groundwater inflow into an underwater tunnel", *Geomech. Eng.*, **20**(3), 267-273. https://doi.org/10.12989/gae.2020.20.3.267.

CC